International Journal of Hydrogen Energy 257 (2026) 156558

Contents lists available at ScienceDirect

International Journal of Hydrogen Energy

journal homepage: www.elsevier.com/locate/he

Environmental footprint of fresh and recycled catalyst production for methane dry reforming

Alessia Amato [a,*], Giulia Merli [a], Alessandro Becci [a], Alessandro Sinopoli [b], Francesca Beolchini [a], Francesco Ferella [c]

[a] Department of Life and Environmental Sciences, Università Politecnica delle Marche, Via Brecce Bianche, Ancona, 60131, Italy
[b] Dipartimento di Scienze Chimiche, Biologiche, Farmaceutiche e Ambientali, Università degli Studi di Messina, Via Stagno d'Alcontres, Messina, 98166, Italy
[c] Department of Industrial and Computer Engineering and Economics, Università degli Studi de L'Aquila, P.le E. Pontieri 1, Monteluco di Roio, L'Aquila, 67100, Italy

ARTICLE INFO

Keywords:
LCA
Methane
DRM
Sustainability
Nickel
Platinum

ABSTRACT

The paper presents an environmental analysis of the production process for a reconditioned catalyst for dry reforming of methane (DRM). This nickel-based catalyst was developed by reformulating a spent catalyst used for carbon monoxide oxidation. The environmental impact of its manufacture was compared with that of a catalyst made from raw materials with the same composition. The life cycle assessment (LCA) showed that the valorization pathway achieved impact reductions in 11 out of 16 categories. Within the adopted system boundaries, limited to catalyst production, the aggregated environmental impacts were reduced by 94% compared to primary production. The catalyst preparation was the main hotspot, driven by nickel precursors (58%) and energy consumption (22%). Sensitivity analysis showed that variations in the electricity mix influences climate change outcomes, while differences in aggregated environmental scores remain limited. These results demonstrate the potential of secondary production as a sustainable and resource-efficient pathway for catalyst manufacturing.

1. Introduction

Methane reforming is a well-established technology to produce hydrogen (H_2) from methane (CH_4). In particular, the steam reforming of methane (SRM) reaction is the most used, especially in oil refining and petrochemical plants.

SRM is based on a multi-tubular reactor, where nickel-based catalysts initiate a vigorous reaction between CH_4 and steam at scorching temperatures exceeding 800 °C to produce synthesis gas (H_2, carbon monoxide (CO), and carbon dioxide (CO_2)). Following this initial reaction, the water-gas shift (WGS) takes place, seamlessly generating additional hydrogen to meet rising demands. The hydrogen produced undergoes purification through pressure swing adsorption (PSA). At the heart of this process there are advanced nickel catalysts, often supported by robust supporting materials like alumina (Al_2O_3), spinel ($MgAl_2O_4$) silica (SiO_2), magnesia (MgO) or their combination. To amplify their effectiveness, promoters such as platinum (Pt), palladium (Pd) of other metals are thoughtfully incorporated, enhancing catalytic activity while minimizing the troublesome issue of coking. In 2023, the global demand for H_2 for all sectors amounted to 97.2 Mton; this amount is expected to grow to nearly 150 Mton by 2030, thanks to the new uses such as power generation, buildings, transportation, and high-temperature thermal energy in industry, in the net zero scenario [1]. However, renewable-based production alone is currently limited by costs and energy requirements. As mentioned, catalysis plays a crucial role in this industrial process; several manufacturers produce SRM catalysts, such as Clariant/Sűd Chemie, Johnson Matthey, Axens, BASF, and Haldor Topsoe. Each company has its own formulations: most of these are Ni-based, like ReforMaxTM 330 LDP (14%wt NiO on $CaAl_{12}O_{19}$, Clariant) and Katalco 57-4Q (18%wt NiO on $CaAl_2O_4$, Johnson Matthey). These types of catalysts are also produced with the addition of K_2O as a promoter, which improves their activity and stability; promoters enhance basicity, boosting CO_2 adsorption and coke gasification, thus significantly reducing carbon deposition and preventing catalyst deactivation. Nevertheless, research never stops trying to find new active metals and compositions, mainly aiming at reducing carbon deposition and poisoning, for instance by H_2S, and prolonging the lifespan, with clear economic advantages.

Nickel-based catalysts are by far the most studied. Typical concentrations of NiO are usually in the range 10-20%wt and must be reduced

* Corresponding author.
E-mail address: a.amato@univpm.it (A. Amato).

https://doi.org/10.1016/j.ijhydene.2026.156558
Received 2 March 2026; Received in revised form 29 June 2026; Accepted 11 July 2026
Available online 15 July 2026

before use to obtain metallic Ni. Activated carbon is one of the possible carriers [2]; other carriers are SiC [3], α-, β-, γ-alumina [4,5], $NiAl_2O_4$ spinel [6], mixed $MgO–Al_2O_3$ [7], hydroxyapatite $Ca_5(PO_4)_3OH$ [8], or $SiO_2–Al_2O_3$ [9]. Some catalysts were synthesized using Ni as an active metal deposited on rare earth elements (REEs) [10]. Other authors investigated the addition of precious metals like Pt as promoter [11,12] on REE carriers [10,13,14].

In addition, the effect of different temperatures, catalyst shapes, and reactor scale-up has been investigated for process optimization and modelling [15–17].

Nevertheless, in recent years, the dry reforming of methane (DRM) has gained attention due to its ability to use CO_2 as a reactant, aligning with decarbonization strategies. The reaction is strongly endothermic:

$$\boldsymbol{CH_4 + CO_2 \leftrightarrow 2CO + 2H_2} \left(\Delta H^0_{298} = 248 \text{ kJ} / \text{mol}\right) \quad \text{[Eq. 1]}$$

Besides that, there are other side reactions to consider in the overall thermodynamic model, such as reverse water-gas shift, methane decomposition, disproportionation of CO, and hydrogenation of CO and CO_2. From the environmental point of view, the process is advantageous as it uses captured CO_2, supporting carbon capture, storage, and utilization (CCSU) policies [18,19].

The advantages, drawbacks, technology barriers, and perspective of the DRM are described in Agun and Abanades [20]. As for SRM, catalyst deactivation and coking are the main problems for DRM catalysts, whereas a key limitation is the constant supply of high-grade CO_2 [20]. Several promoters, including K, are proposed for DRM catalysts [21].

The catalysts used for DRM are very similar to those used for steam reforming, with nickel as the main active metal on various supports [22–31]. Carbon-based catalysts have been extensively synthesized and tested [31].

Recently, there has been increasing attention towards the possibility of reforming biogas, which contains around 50%vol of CH_4 [32,33]. The best conversion results, obtained at 750 °C, show CH_4 conversion yields of 83-99% and CO_2 reaction rates of 92-98% [24,26,29].

On a larger scale, industrial-scale DRM projects are being developed (e.g. LG Chem in South Korea), using CO_2 and CH_4 to produce syngas within carbon capture and utilization schemes [34]. The new process will reduce the reliance on coal.

In Europe, there is a pilot plant developed at Ghent University, named “Superdry Reforming (SDR)”, which can convert 1 kg of CO_2 per hour. The innovation lies in the fact that the process can convert three times as much CO_2 per unit of CH_4 [35].

Nevertheless, the idea of reusing spent catalysts for other catalytic processes was already demonstrated with spent fluid catalytic cracking catalysts (FCCCs), which were reused for DRM after impregnation with nickel. The final CH_4 and CO_2 conversion was in the 40-60% range [36].

Life cycle assessment (LCA) has recently been applied to methane reforming technologies, including DRM, to explore the environmental implication of using CH_4 and CO_2 as feedstock for syngas or hydrogen production [37,38]. These studies consistently show that the energy supply and feedstock choice strongly influence the overall carbon footprint [38]. However, existing LCA works mainly focus on process configuration and energy integration, while the role of catalysts is simplified, often limited to their initial production, with regeneration and end-of-life stages generally excluded from the system boundaries [37]. Evidence from LCA works on catalyst recycling and regeneration in other catalytic applications show that extending catalyst lifetime can substantially lower environmental burdens [39–41]. However, such approaches have not yet been systematically applied to DRM systems, highlighting a clear gap that this study aims to address.

In this paper, an LCA study is performed on a Ni-based DRM catalyst obtained from a reformulated spent Pt-containing catalyst, promoting reuse before metal recovery.

The outcomes of this paper comply with the Sustainable Development Goal (SDG) n. 7 as DRM generates a blue H_2 as a transition energy vector [42,43]. Furthermore, they match the SDG n. 13, as DRM will use captured CO_2 in the CCSU chain, contributing to concrete actions that counter the climate change.

2. Description of the production process

The Ni-based catalyst for DRM was synthesized from a spent catalyst used in a thermochemical plant fuelled by natural gas to oxidize CO. The catalyst is arranged in corrugated metallic sheets held together by a 600x600 × 100 mm metal frame. The active layer was deposited on these sheets; it was therefore manually scratched, and the powder was used as a carrier for the downstream synthesis stages. The sheets and the removed powder are shown in Fig. 1. The synthesis method to produce the DRM catalyst is detailed in Abotaleb et al. [44].

The flow-sheet of the manufacturing plant is reported in Fig. 2. The facility works in batch mode, completing 137 processing cycles per year, each one lasting nearly two days. A reasonable target was indeed established to collect 10,000 catalytic modules annually, which corresponds to catalysts from 10 to 15 plants. 205 t/y of spent oxiCO catalyst (steel modules) are treated, yielding about 16.4 t/y of catalytic layer for subsequent synthesis. Accordingly, the nominal throughput of the hydro-synthesis section is 120 kg per batch [44].

Module dismantling is planned for over two months, during which the catalytic layer is separated from the sheets for Ni/DRM catalyst production. This operation also generates 145 ton/y of metal sheets made of the FeCrAl Kanthal alloy and 44 ton/y of steel frames (AISI 304), which can obviously be valorized. The catalyst lifetime in thermochemical plants, incinerators, and steelmaking plants is 2-3 years, depending on the fuel type and operational conditions.

The recoverable platinum in the catalytic layer was determined at 4700 mg/kg. Hence, the overall Ni/DRM catalyst produced annually amounts to 16.2 tons.

The mass balance is derived from laboratory-scale experiments. All process units are equipped with an automated monitoring and control architecture that maintains operating variables at their predefined setpoints. Instrumentation, valves, and control elements are integrated within a distributed control system (DCS), which provides real-time visualization of the main process parameters in the control room. The Ni/DRM catalyst production facility can be conceptually divided into three main sections: (i) physico-mechanical pretreatment operations aimed at separating the catalytic layer from the spent oxiCO catalysts and preparing it for deposition; (ii) synthesis of the Ni/DRM catalyst; and (iii) wastewater and flue-gas treatment.

2.1. Pre-treatment section

The modules collected from power generation facilities are transported to the processing plant and stored in a protected building, given the high economic value of platinum. Each module undergoes manual disassembly: the external frame is cut, and the metal plates bearing the catalytic coating are readily separated and collected in barrels. The frames are temporarily stored outdoors under a sheltered area for subsequent recycling, while the barrels containing the metal plates are conveyed to the crushing unit. The jaw crusher (JC-01 in Fig. 2) compresses the plate-shaped sheets, minimizing milling effects and consequently limiting the release of ferroalloy. As a result, the $Al_2O_3–La_2O_3$ ceramic catalytic layer containing platinum detaches from the metal substrate and is collected at the conical discharge section, which is fitted with a 1 mm sieve. The recovered catalytic material is subsequently stored in barrels.

The crushing process is conducted in batch mode, with the residence time adjusted to ensure the removal of at least 95% of the total catalytic layer mass. Following crushing, the stripped metal sheets are extracted from the crusher and stored in a separate covered area, reflecting their different economic value compared to the frames.

Finally, 120 kg of the recovered catalytic material are charged into a

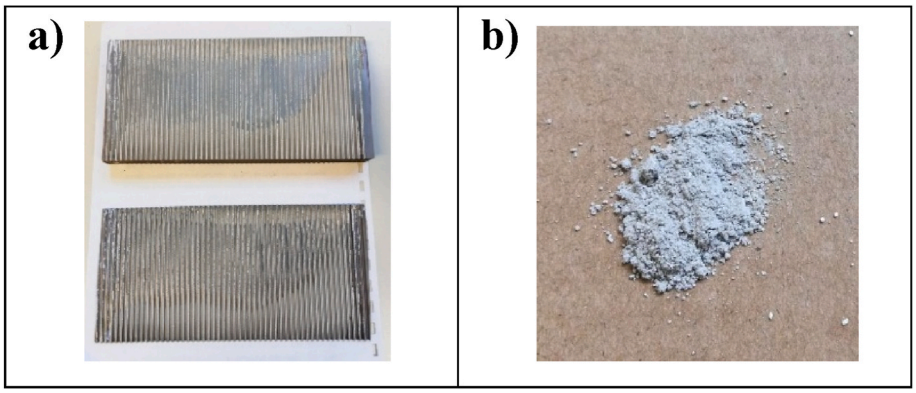

Fig. 1. – Metal sheet pieces (a), and catalytic layer powder (b).

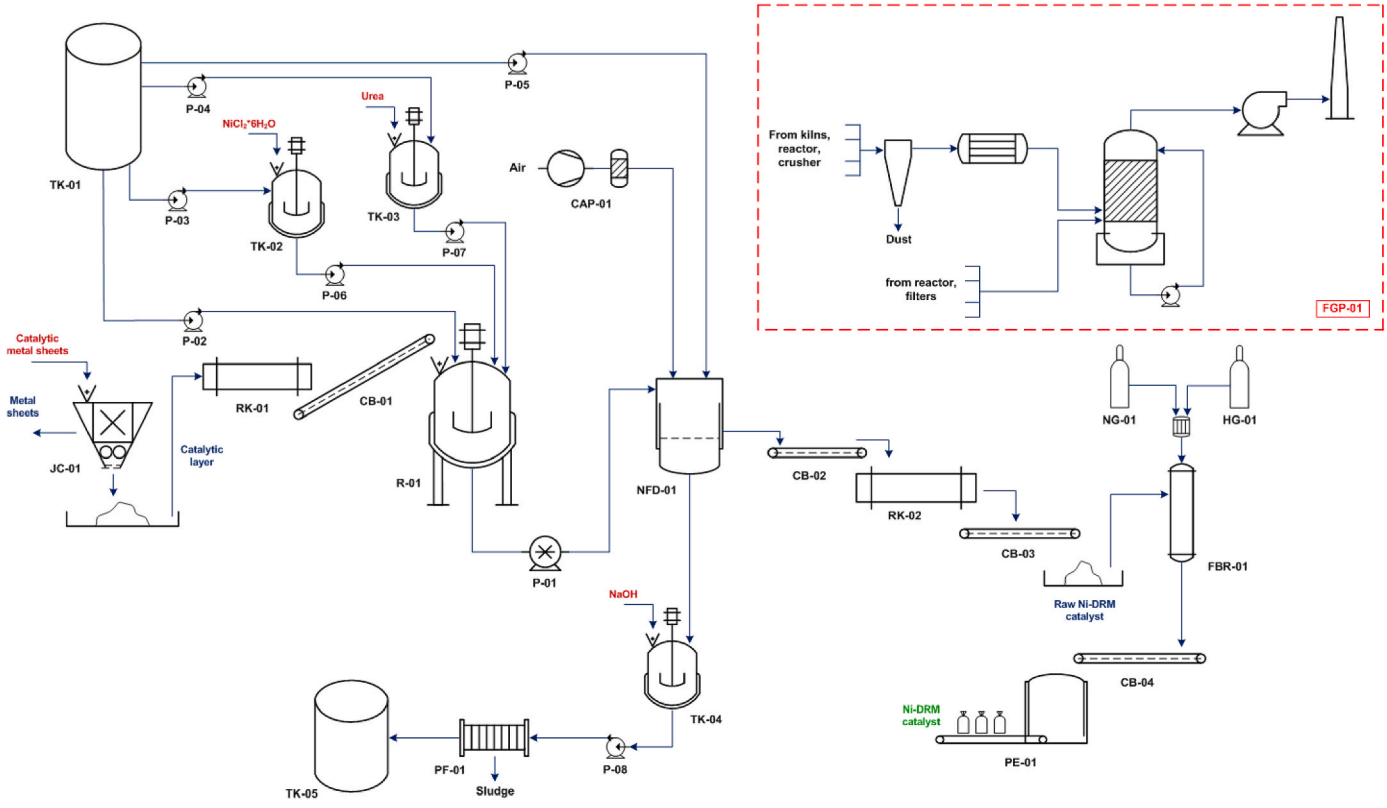

Fig. 2. – Flow-sheet of the plant for the recycling of the oxiCO spent catalyst.

rotary kiln (RK-01), where oxidative treatment is performed at 600 °C for 1 h to eliminate residual carbonaceous species and hydrocarbons. After roasting, the material is discharged onto a covered conveyor belt (CB-01) and cooled to 50 °C before being transferred to the reactor (R-01), where the nickel deposition step is initiated.

2.2. Ni/DRM catalyst synthesis section

Six cubic meters of demineralized water are fed into the reactor from tank TK-01 using pump P-02, and the resulting suspension is agitated for 1 h at ambient temperature. Subsequently, 2.4 m^3 of an aqueous $NiCl_2{\cdot}6H_2O$ solution (20 g/L) are gradually introduced over 6 h at room temperature via a metering pump (P-06). This solution is prepared in a stirred vessel (TK-02), where demineralized water delivered by pump P-03 is combined with solid nickel chloride under intense mixing.

Thereafter, 1.2 m^3 of a urea solution (100 g/L) are added slowly within 30 min. The mixture is then heated to 90 °C and maintained under continuous stirring for 10 h to complete the deposition process. At the end of this stage, the suspension is transferred by pump P-01 to a Nutsche filter-dryer (NFD-01), which was selected to integrate filtration and drying in a single unit.

Filtration is performed by pressurizing the headspace of NFD-01 with compressed air. Once filtration is complete, 3.4 m^3 of water are introduced to wash the filter cake; this washing cycle is repeated to ensure the complete removal of residual nickel-containing solution from the solid phase.

The washed cake is subsequently dried in the Nutsche filter-dryer and sent via a belt conveyor (CB-02) to a rotary kiln (RK-02). The resulting Ni/DRM precursor catalyst is calcined at 800 °C for 6 h under an air atmosphere. After calcination, the kiln is discharged, and the material is partially cooled on a conveyor belt (CB-03) prior to the final treatment step. Since nickel is present as oxide species (NiO and Ni_2O_3),

a reduction step is required. This is carried out in a fixed-bed reactor (FBR-01) at 750 °C for 1 h using a 5% hydrogen-nitrogen gas mixture.

Nitrogen is generated on-site using a pressure swing adsorption unit (NG-01), as this option is more economical than importing compressed gas cylinders and represents a cost-effective alternative to argon. Hydrogen, by contrast, is supplied in pressurized cylinders, given the relatively limited annual consumption.

Following reduction, the fixed-bed reactor is unloaded, and the Ni/DRM catalyst is cooled on a conveyor belt (CB-04) before being packaged in 25 kg bags and placed into barrels using the packaging equipment PE-01.

2.3. Flue-gas and waste solution treatment sections

The spent solution and the washing effluents from the Nutsche filter are collected in a mixing vessel (TK-04), where solid sodium hydroxide is added until the pH reaches 8. Under these conditions, dissolved metals precipitate in the form of hydroxides, and the resulting sludge is separated by filtration using a plate-and-frame filter press (PF-01), to which the suspension is delivered by pump P-08. The clarified filtrate is transferred to tank TK-05 and subsequently discharged into the industrial park sewer system for downstream wastewater treatment.

Dust generated during mechanical pretreatment operations and from the rotary kilns is treated using a cyclone separator, allowing the recovery of particulate matter containing platinum. The cleaned flue gas stream is then cooled in a gas–gas heat exchanger. Downstream of this unit, a wet scrubber removes condensable vapors from both the cooled flue gas and the exhaust from reactor R-01, in which partial water evaporation occurs at 90 °C. The treated gas is finally conveyed by the main fan to a cooled stack for atmospheric discharge. The entire gas handling and abatement train constitutes the flue gas processing section (FGP-01).

The utility systems include a compressed air package (CAP-01) supplying both process and instrument air, a boiler (BO-01) providing steam for heating reactor R-01 and for drying the filter cake in NFD-01, and a nitrogen generation unit (NG-01).

3. Materials and methods

3.1. LCA system boundaries

The production of Ni-DRM catalyst, based on the recycling process described in paragraph 2, was evaluated through the LCA analysis (Scenario 1) and compared with the primary production of the same product based on the exploitation of virgin raw materials (Scenario 2). Scenario 2 represents the conventional reference route for catalyst manufacture, in which all materials recovered in scenario 1 are supplied from primary source. For each material considered, the selected database dataset includes the full upstream supply chain, including resource extraction, refining, industrial processing, transport as well as the associated material and energy inputs and related emission.

In accordance with the methodological hierarchy established by ISO standards, metallic components separated during dismantling (metals sheets and steel frames), although potentially reusable, were excluded from both scenarios to avoid allocation procedures not relevant to the goal of the study. The assessment was therefore limited exclusively to catalyst production. The use phase was not included, assuming comparable catalytic function under equivalent operating conditions. Within the system boundaries, Pt is treated as part of the catalyst matrix rather than as a separate co-product; therefore, no allocation procedure is applied, as suggested by ISO standard 14044 [45]. The Pt content used in the inventory corresponds to the recoverable platinum in the catalytic layer (4700 mg/kg) [44].The system boundaries of the two processes are reported in Fig. 3. Concerning scenario 1, all process water streams are sent to the wastewater treatment unit and subsequently recycled within the system. Accordingly, only the operational inputs associated with

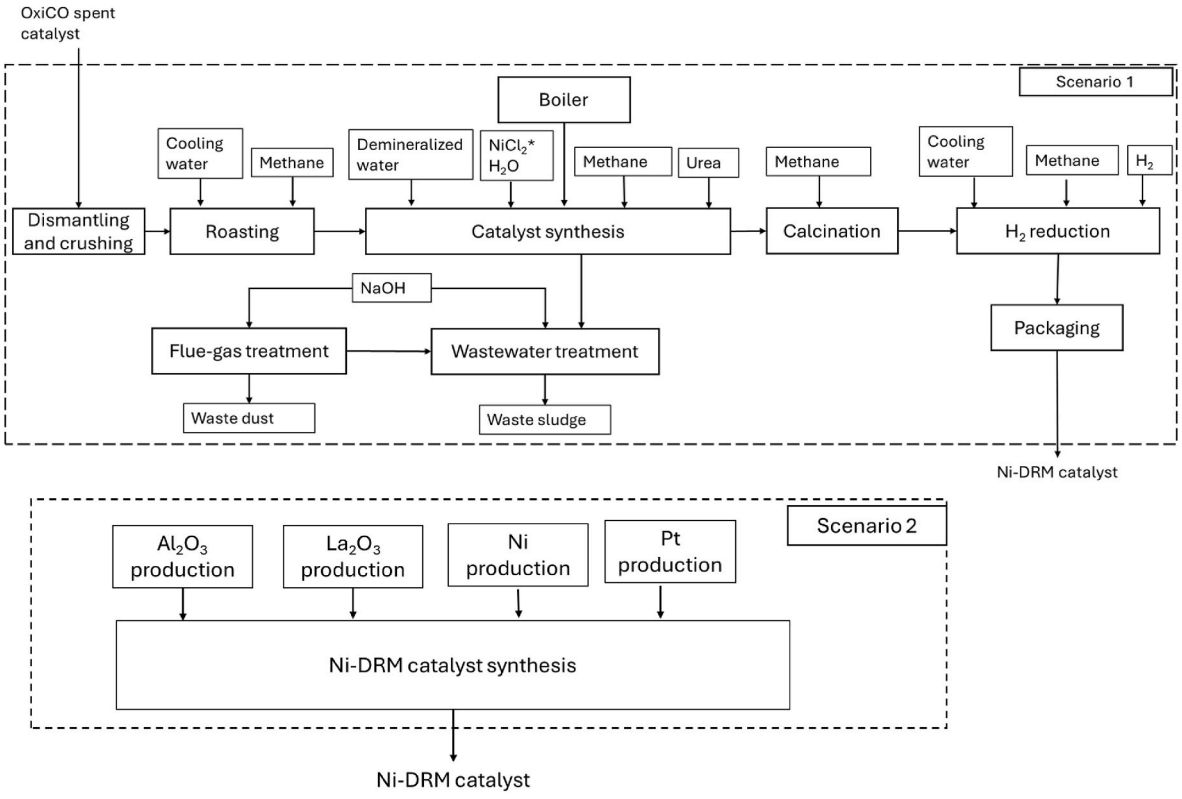

Fig. 3. System boundaries of Ni-DRM catalyst production through recycling (scenario 1) and from virgin raw materials (scenario 2). The corresponding energy demand for each process stage was also included in the assessment, despite not being explicitly represented in the diagram.

wastewater treatment and the make-up water (deionised water and cooling water) required to compensate evaporation losses are considered in the LCA model. Furthermore, although not explicitly shown in the system boundaries, the energy required by each process unit was included in the LCA model, as reported in the life cycle inventory.

3.2. Life cycle inventory (LCI)

To provide a complete representation of the process inputs and outputs, mass and energy balances were developed to perform the LCA (Tables 1 and 2). The functional unit was defined as 16,200 kg of Ni-DRM catalyst, corresponding to the annual production capacity of the innovative recycling process. Since the study compares alternative production routes for the same catalyst formulation intended for the same dry reforming application, a mass-based functional unit was adopted, assuming equivalent catalytic functionality between the recycled and conventional Ni-based DRM catalyst. This assumption is supported by the experimental results reported by Abotaleb et al. [44], where the recycled catalyst exhibited stable performance under DRM conditions, maintaining CH_4 and CO_2 conversions above 70% and 89% (up to 94%), respectively, with negligible deactivation over 7 h of continuous operation. These findings support the assumption that the recycled catalyst provides the intended catalytic function for comparative LCA. The main assumptions considered for the LCI were reported below. The inventory for primary catalyst production was developed by combining stoichiometric precursor requirements with specific background dataset from Sphera database. For the modelling of scenario 2, the Ni-DRM catalyst composition was reconstructed from the catalyst preparation procedure described in a previous study [44] and expressed as 85.94 wt% Al_2O_3, 3.92 wt% La_2O_3, 0.49 wt% Pt, and 9.65 wt% Ni.

Table 1
– Detailed LCI of scenario 1 (recycling route)[a].

OPERATION	INPUT	OUTPUT
Dismantling and crushing		
Electrical energy (kWh/y)	4129	
OxiCO spent catalyst (kg/y)	16,200	
Roasting		
Electrical energy (kWh/y)	1048	
Methane (Nm3/y)	4697	
Cooling water (make-up) (kg/y)	109,600	
Catalyst synthesis		
Electrical energy (kWh/y)	244,442	
Demineralized water (kg/y)	1200	
Methane (Nm3/y)	24,829	
$NiCl_2$•6H2O (kg/y)	6439	
Urea (kg/y)	16,440	
Ni-DRM catalyst (kg/y)		16,200
Calcination		
Electrical energy (kWh/y)	1404	
Methane (Nm3/y)	35,535	
H_2 reduction		
Electrical energy (kWh/y)	1219	
Methane (Nm3/y)	3269	
Hydrogen (Nm3/y)	2570	
Cooling water (make-up) (kg/y)	137,000	
Wastewater treatment		
Electrical energy (kWh/y)	4644	
NaOH (kg/y)	6850	
Waste sludge (kg/y)		12,330
Packaging		
Electrical energy (kWh/y)	6165	
Fuel gas treatment		
Electrical energy (kWh/y)	40,552	
NaOH (kg/y)	1370	
Waste dust (kg/y)		274
Boiler		
Electrical energy (kWh/y)	4110	

[a] FeCrAl alloy and stainless-steel frame were excluded from the system boundaries; therefore, the associated environmental burdens and credits were not considered in the LCA.

Table 2
– LCI of scenario 2 (primary production route).

PRIMARY PRODUCTION	INPUT	OUTPUT
Al_2O_3 (kg/y)	13,923	
La_2O_3 (kg/y)	635	
Pt (kg/y)	79	
Ni (kg/y)	1563	
Ni-DRM catalyst (kg/y)		16,200

Each precursor was linked to its corresponding industrial production dataset (e.g. global production of platinum group metals) The full list of datasets adopted for raw materials is reported in the supporting materials (Table S1).

Unit process data for nickel chloride hexahydrate ($NiCl_2{\cdot}6H_2O$) were not available in the databases used, therefore, the impact of the salt was estimated by reconstructing its synthesis from Ni, HCl and H_2O, according to the mechanism described by Gad [46], through the following reactions:

$$Ni\ (s) + 2\ HCl\ (aq) \rightarrow NiCl_2\ (aq) + H_2\ (g) \quad \text{[Eq. 2]}$$

$$NiCl_2\ (aq) + 6H_2O \rightarrow NiCl_2{\cdot}6H_2O\ (s) \quad \text{[Eq. 3]}$$

The resulting impact was calculated as the weighted sum of the unit impacts of these precursors. The reconstructed inventory for nickel chloride was cross-checked against literature data reported by Affranchi et al. [47], where it was identified as a relevant environmental hotspot, confirming a comparable order of magnitude for the climate change category impact.

Cooling water is assumed to be recirculated, and is therefore modelled as make-up water only, corresponding to 20% of the total flow, which is included in the inventory as net consumption for roasting and H_2 reduction steps. Demineralized water is also included as make-up and is modelled using a dataset that accounts for the impact of the demineralization process (e.g. reverse osmosis).

Nitrogen used in the reduction step is generated on-site from compressed air via PSA and is not included as a separate input in the LCI, its environmental impact is accounted for through the associated electricity consumption. However, this study represents a first estimate of the environmental benefits of the DRM, but a more accurate estimate of the data would certainly require the tests at a pilot scale before one can invest in a full-scale plant.

3.3. Study limitations

The results of this study should be interpreted considering the adopted system boundaries and the assumptions used for inventory modelling. First, the assessment was limited to the catalyst production stage and did not include the catalyst use phase or its end-of-life management, common to both the scenarios. Therefore, functional equivalence between the recycled catalyst and a conventional Ni-based DRM catalyst was assumed, based on the experimental evidence reported by Abotaleb et al. [44]. Furthermore, FeCrAl alloy sheets and the stainless-steel frame recovered during catalyst dismantling were excluded from the system boundaries; consequently, no environmental burdens or credits associated with these recovered materials were considered. In addition, part of the life cycle inventory was reconstructed from laboratory-scale experimental data and stoichiometric calculations. Nevertheless, the sensitivity analyses performed in this study support the robustness of the overall conclusions.

3.4. Software and methods

The life cycle assessment was performed in accordance with the principles and framework of ISO 14040 and ISO 14044 standards [45, 48]. The LCI was developed within a single modelling framework using

LCA for Experts software by Sphera. Background datasets were primarily sourced from Sphera Professional Database (My Professional Database 2024.2). When equivalent processes were not available, complementary datasets were selected from the Ecoinvent database (accessed via SimaPro). Only three background datasets were taken from the Ecoinvent database, as reported in Table S2. To ensure methodological consistency, all datasets were implemented within the same modelling framework and harmonized by adopting a consistent cut-off approach. The same life cycle impact assessment method was applied to all inventory flows regardless of their database origin. Impact assessment was

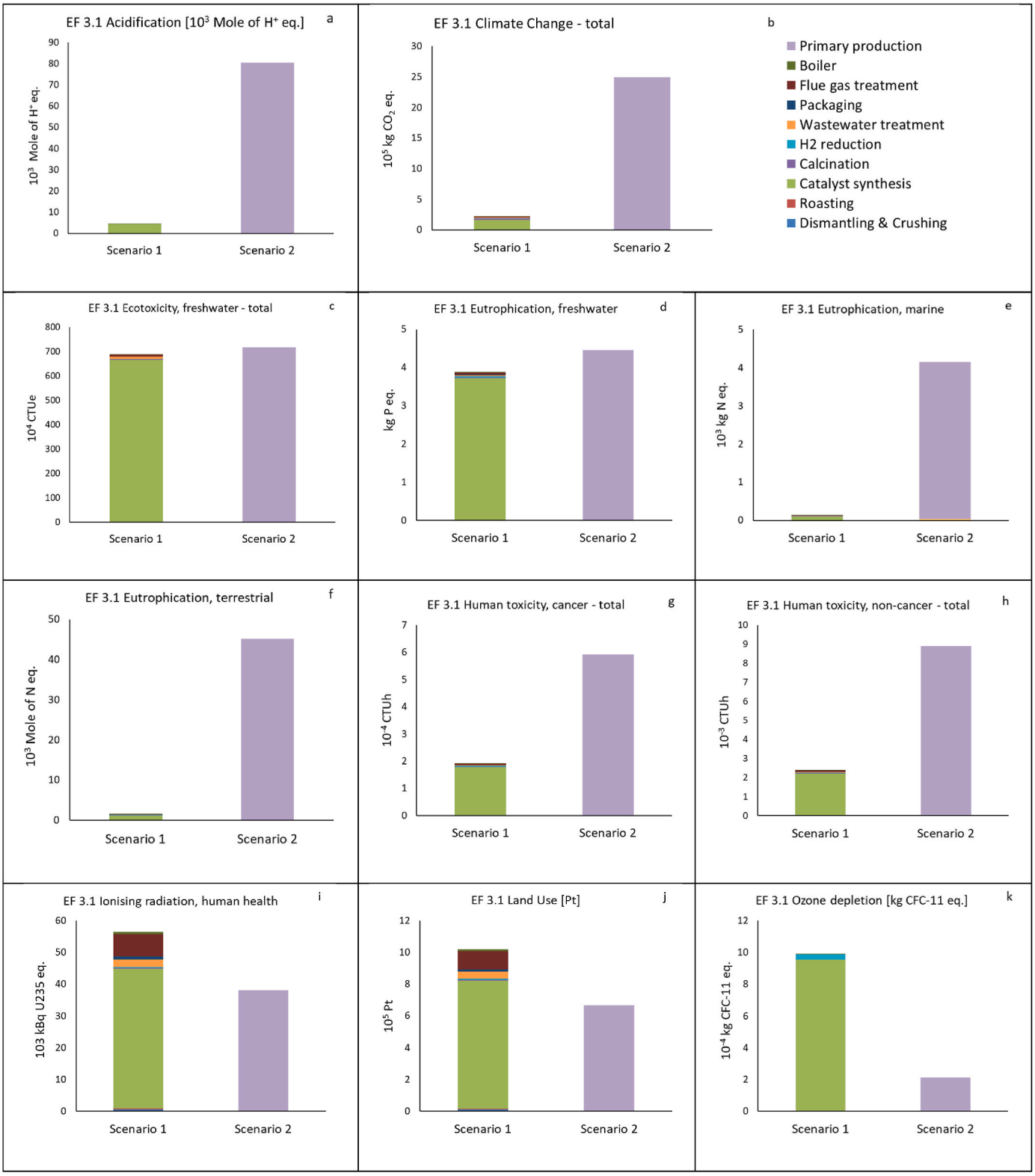

Fig. 4. Environmental impact assessment results for catalyst production via recycling and primary production from raw materials (functional unit: 16,200 kg of Ni-DRM catalyst).

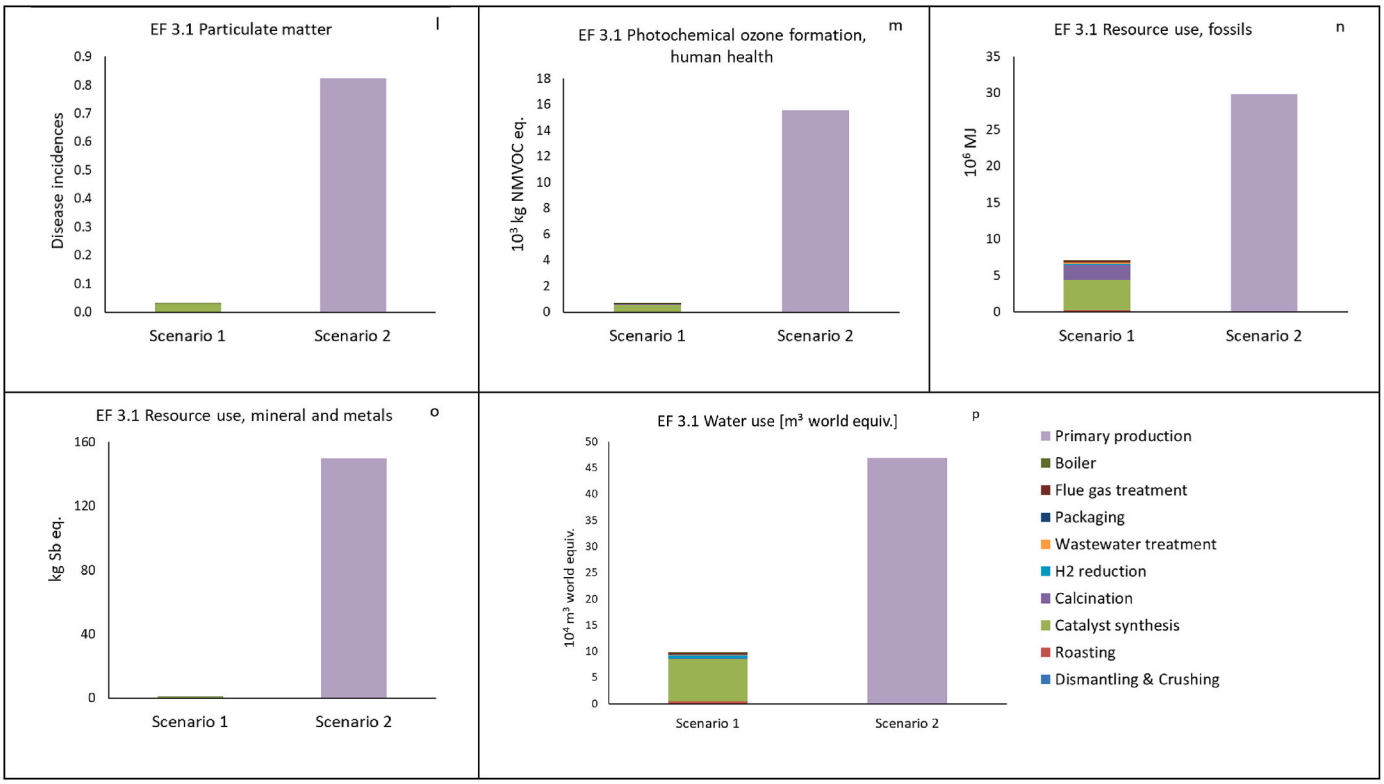

Fig. 4. (*continued*).

carried out using the Environmental Footprint (EF) 3.1 method, in which inventory flows are classified into the relevant impact categories and converted into category-specific impacts. Normalization and weighting phases were applied to support comparison and interpretation of the results. The results of normalization and weighting were reported in person equivalent (p.e.), which represent the number of average European citizens whose annual environmental burdens correspond to the assessed impacts [49].

4. Life cycle impact assessment results and discussion

4.1. Classification and characterization phase

For the LCA study, the secondary catalyst production process, divided into individual process blocks, was compared with the primary production of the catalyst starting from raw materials. As shown in Fig. 4, the process under analysis appears overall more sustainable than the primary production of the same amount of product. In 11 out of 16 impact categories, the impacts associated with primary production from raw materials are more than twice those related to the production of the same products through the investigated process. This result is mainly associated with the avoidance of primary platinum production, which represent the dominant contribution to most impact categories in the conventional production scenario, while alumina provides a secondary contribution. The remaining five categories (Fig. 4c, d, i, j and k), in which the impact of the process is higher or comparable to scenario 2, indicate that the most environmentally impacted process block is "Catalyst synthesis".

The "Catalyst synthesis" process block was therefore analysed in greater detail for the impact categories with the highest environmental relevance, to identify the main contributing factors. The analysis shows that each impact category is dominated by flows consistent with their environmental nature. In the case of *ecotoxicity, freshwater* (Fig. 5a), the main contribution is the use of the reagent $NiCl_2 \bullet 6H_2O$, as nickel being a heavy metal exhibits high environmental toxicity and is associated with harmful effects on both terrestrial and aquatic organisms. Urea contributes significantly to the *eutrophication, freshwater* and *ozone depletion* categories (Fig. 5b and e). In the former case, this is due to its high nitrogen content, which may be released as nitrates or ammonium, the main drivers of eutrophication processes. In the latter case, the impact is related to upstream processes associated with industrial ammonia production. *Ionising radiation* and *land use* categories (Fig. 5c and d) are mainly affected by electricity consumption, depending on the composition of the energy mix and the infrastructure required for electricity generation. The electricity mix used is the European electricity mix, which is characterized by combination of fossil fuels, nuclear power and renewable sources.

Anyway, scenario 2 shows higher impacts in the *ecotoxicity, freshwater* and *land use* categories (Fig. 4c and j), as it includes the extraction and refining stage of alumina, rare earth elements and noble metals, which are well known to involve high land occupation and emission of metals and residues with high toxic potential.

4.2. Normalization and weighting phase

The normalization and weighting phase resulted in a total score of 35 p.e. for the analysed process versus 548 p.e. for the primary production scenario. Within the adopted system boundaries, corresponding to catalyst production, this represents an aggregated impact reduction of approximately 94% (Fig. 6a). According to the applied weighting method, this indicates that the process is substantially more sustainable than the raw materials-based scenario. The dominant impact categories for scenario 1 after normalization and weighting are *resource use, fossils* (27%), *climate change* (23%), *acidification* (14%), *particulate matter* (13%) and *ecotoxicity, freshwater* (9%). These results integrate those obtained at the characterization stage, since normalization scales each impact against a global reference, while weighting assigns relative importance based on environmental or societal relevance. As a result, categories such as *climate change* and *resource use, fossils* become predominant, indicating that the overall environmental burden of the

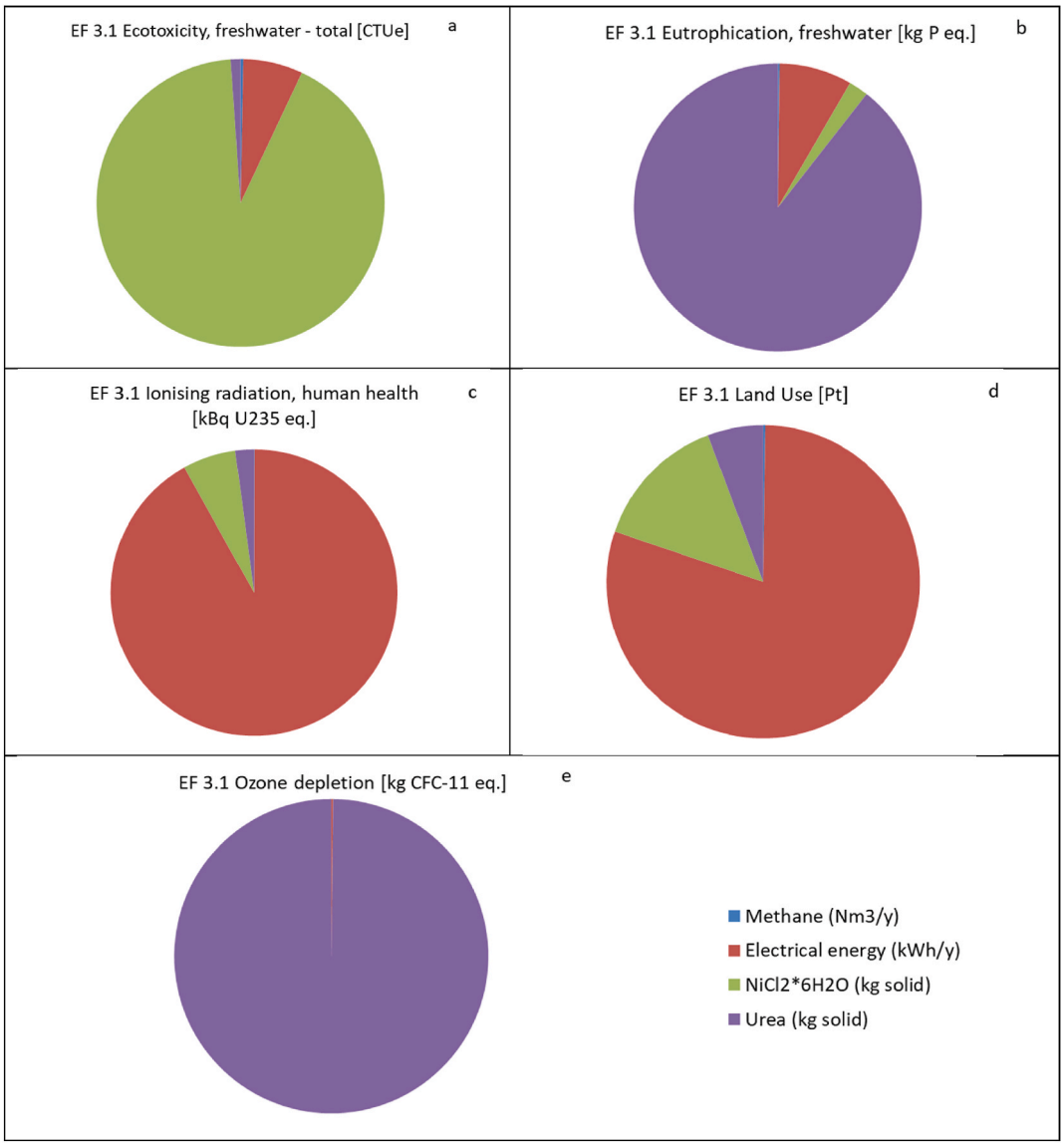

Fig. 5. Analysis of the impact of individual factors during the classification and characterization phase for the most impactful categories in scenario 1.

process is mainly driven by energy consumption and upstream emission rather than by the direct toxicity of the chemicals involved.

By analysing the process blocks, the results confirm what was reported in characterization and classification, where the most impactful block appears to be the catalyst synthesis process (Fig. 6b). In light of this, a further contribution analysis was carried out, focusing on the inputs associated with this block. The normalization and weighting results show that, within the catalyst synthesis process, 58% of the aggregated impact is attributable to the reagent $NiCl_2 \bullet 6H_2O$, 22% to electricity and 10% to both methane and urea (Fig. 6c). This indicates that the overall environmental burden is dominated by the nickel-containing reagent, suggesting that strategies to optimize its use and recover of any unreacted material could significantly reduce environmental impacts.

A sensitivity analysis was performed by varying the consumption of $NiCl_2 \bullet 6H_2O$ by ±30%, since this inventory flow was estimated from laboratory scale and stoichiometric calculations. The normalized and weighted score ranged from 31.0 p.e. (−30%) to 39.8 p.e. (+30%), compared with 35.4 p.e. for the base case. These values correspond to overall impact reduction of 92.6% and 94.2%, respectively, compared with the primary catalyst production scenario (548 p.e.), confirming the robustness of conclusions despite $NiCl_2$ inventory uncertainty.

4.3. *Sensitivity analysis*

Although the inventory was reconstructed from laboratory-scale data, industrial implementation may lead to changes in process performance. On the one hand, process scale-up is generally associated with improved energy efficiency and reduced reagent consumption through process optimization, potentially leading to further reductions in environmental impact [50–52]. On the other hand, industrial operation may also affect the recovery efficiencies achieved under laboratory conditions. Although these aspects were not explicitly evaluated in the present study, the substantial environmental advantage observed for the recycling process over primary catalyst production suggests that the overall environmental benefit would likely be maintained. To further evaluate the robustness of the environmental assessment, sensitivity analysis was performed on selected modelling assumptions.

Energy consumption represents one of the main environmental hotspots in industrial and laboratory processes, particularly influencing climate change impacts. In the present case, energy demand represents the second most relevant contribution, accounting for 19% of the total impact. The environmental impact of electricity consumption, however, depends not only on the amount of energy used, but also on the composition of the electricity mix.

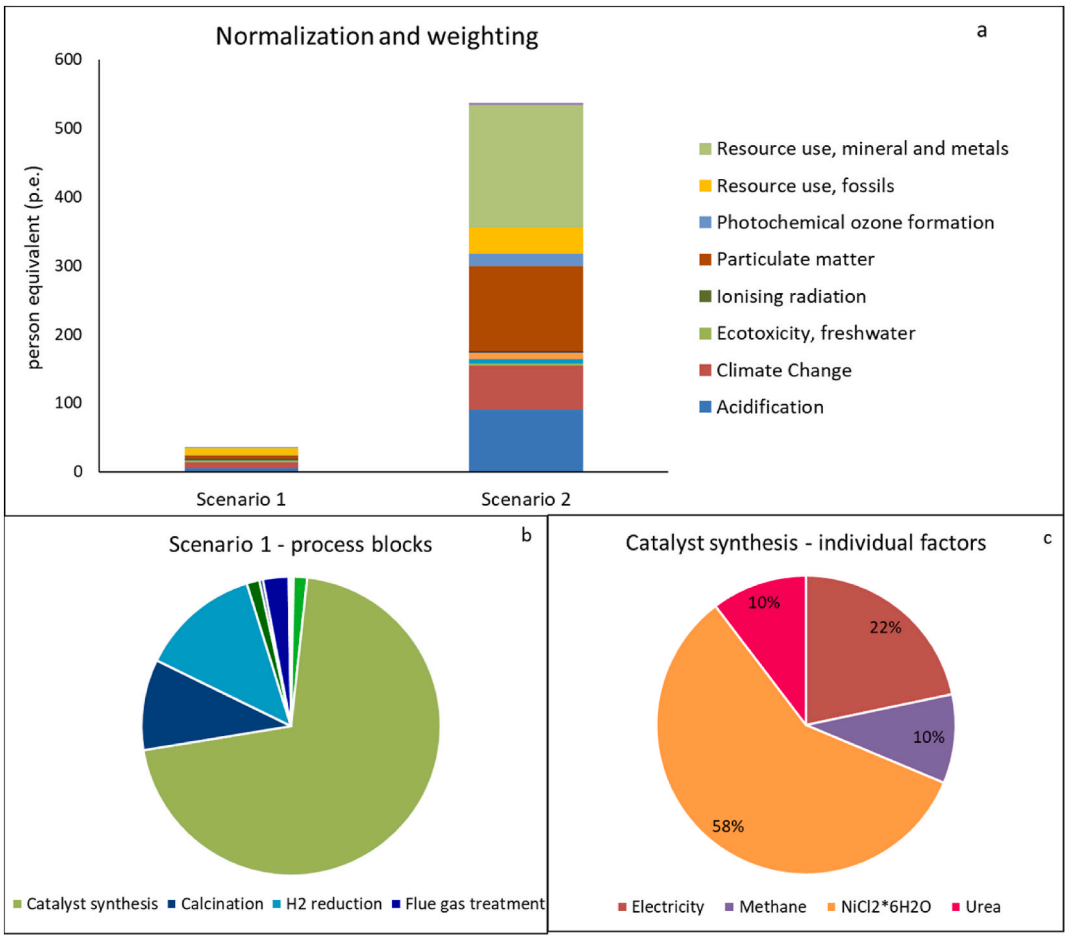

Fig. 6. Results of normalization and weighting steps (expressed as person equivalent). Comparison between the two considered scenarios, where the pie-chart on the top reports the contribution on impact category mainly affected for scenario 1 (a). Details of scenario 1 most impacted process blocks (b) and input contribution within the catalyst synthesis block (c). Charts legends report only the categories with impact greater than 3%.

To assess the robustness of the results, a sensitivity analysis was performed considering three different electricity supply scenarios: the European mix, the Ontario (Canada) mix and a completely photovoltaic scenario. In this context, the comparison among three different energy supply options does not aim to assess the effect of the electricity source selection on the overall process impact. Rather, this aspect is considered relevant in order to support and guide the choice of plant location. In this regard, the European mix includes a relevant share of fossil fuels, while Ontario mix was selected as a low-carbon scenario, as it is predominantly based on nuclear and hydropower, with a limited contribution from fossil fuels. The photovoltaic scenario, on the other hand, is characterized by negligible operational emission, with impacts mainly

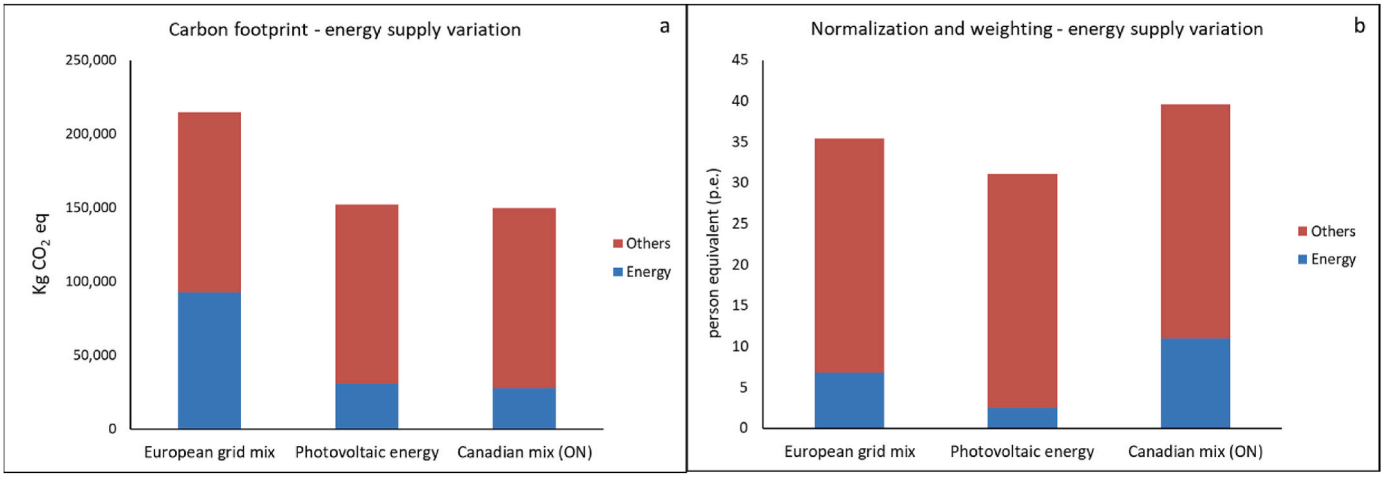

Fig. 7. Sensitivity analysis of the process under different electricity mixes: carbon footprint (a) and normalized and weighted impacts (b). "Others" is the sum of the impacts of methane, cooling water, $NiCl_2 \bullet 6H_2O$, urea, hydrogen, NaOH, hazardous waste, which is constant among the scenarios.

related to the production, installation and end-of-life of the panels. In this scenario, however, only electricity was assumed to be fully supplied by photovoltaic energy, whereas thermal energy was modelled using the conventional European mix. Within the LCA framework, Carbon Footprint analysis is used as the reference indicator for climate change impact and is expressed in kg CO_2 eq. The results of this analysis show higher climate change impacts for the European mix, while low-carbon scenarios significantly reduce CO_2 emissions (Fig. 7a). The carbon footprint of the two low-carbon scenarios is similar, since in the photovoltaic scenario the benefit of using photovoltaic electricity for the electrical demand only is partially masked by the contribution from thermal energy use (Fig. 7a). However, after normalization and weighting, according to Environmental Footprint 3.1 method, the Ontario mix shows the highest overall environmental impact due to increased contribution in non-climate categories (such as human toxicity, ionising radiation, and freshwater eutrophication) (Fig. 7b). A similar trend can already be observed at the normalized (non-weighted) level (Table S3, supporting materials), indicating that these differences are inherent to the environmental profiles of the electricity mixes rather than solely a result of the weighting step. Conversely, the photovoltaic scenario results in the lowest aggregated environmental impact (Fig. 7b). Overall, the sensitivity analysis indicates that a reduction in carbon footprint does not necessarily correspond to a reduction in total environmental impact, confirming the relevance of multi-category LCA approach and supporting the robustness of the results with respect to electricity supply assumptions. Increasing the share of photovoltaic electricity has the potential to reduce the environmental impacts, but it provides only a limited additional improvement to the performance of the analysed process.

5. Conclusions

This study assessed the environmental performance of a Ni-based catalyst for DRM obtained through the valorization of a spent catalyst, comparing it with a conventional primary production scenario based on raw materials extraction and refining. The results demonstrate that recovering and reprocessing the spent material represents a significantly more sustainable alternative, with lower impacts across most categories and a substantial reduction in the aggregated environmental score after normalization and weighting (with an environmental gain exceeding 90%). These findings highlight the strong environmental relevance of avoiding extraction and refining stages, which are major contributors to ecotoxicity, land use, and overall resource-related impacts.

Within the analysed system, the catalyst synthesis block represents the primary hotspot, with nickel-containing reagent dominating the overall impact. Nickel is essential for catalyst activity; however, careful management of its use could further reduce environmental impact. Energy demand, particularly electricity consumption, is a significant contributor to climate change and resource use categories, highlighting the importance of exploring low-carbon alternatives. Sensitivity analysis across different electricity supply scenarios demonstrates that the overall sustainability of the process is robust, and that although low-carbon or photovoltaic electricity can further lower the carbon footprint, they do not necessarily translate into a proportional decrease in the total environmental burden. These results underline the importance of a multi-category LCA approach when evaluating emerging processes. Overall, the proposed process offers clear environmental advantages over primary production, while also identifying specific priorities for further optimization.

Funding

This research did not receive any specific grant from funding agencies in the public, commercial, or not-for-profit sectors.

CRediT authorship contribution statement

Alessia Amato: Conceptualization, Investigation, Methodology, Software, Validation, Writing – review & editing. **Giulia Merli:** Data curation, Formal analysis, Investigation, Visualization, Writing – original draft. **Alessandro Becci:** Formal analysis, Software. **Alessandro Sinopoli:** Data curation, Formal analysis, Investigation, Visualization, Writing – original draft. **Francesca Beolchini:** Methodology, Software. **Francesco Ferella:** Conceptualization, Formal analysis, Funding acquisition, Investigation, Project administration, Resources, Supervision, Validation, Visualization, Writing – original draft, Writing – review & editing.

Declaration of competing interest

The authors declare that they have no known competing financial interests or personal relationships that could have appeared to influence the work reported in this paper.

Appendix A. Supplementary data

Supplementary data to this article can be found online at https://doi.org/10.1016/j.ijhydene.2026.156558.

References

[1] IEA. Global hydrogen demand by sector in the net zero scenario, 2020-2030. Paris: IEA; 2026. https://www.iea.org/data-and-statistics/charts/global-hydrogen-demand-by-sector-in-the-net-zero-scenario-2020-2030-2. [Accessed 26 January 2026].
[2] Zulqarnain Nabila R, Rudly C, Noh Y, Kim S, Chun D, et al. Nickel catalysts supported on activated carbons with tunable pore structure for methanol steam reforming and CO2 methanation. J Ind Eng Chem 2025. https://doi.org/10.1016/j.jiec.2025.11.024.
[3] Shen Z, Nabavi SA, Clough PT. Intrinsic kinetics of steam methane reforming over a monolithic nickel catalyst in a fixed bed reactor system. Chem Eng Sci 2024;299:120482. https://doi.org/10.1016/j.ces.2024.120482.
[4] Shigarov AB. Approximate calculation of the apparent reaction rate of methane steam reforming on an industrial nickel catalyst for time-efficient computations. Int J Hydrogen Energy 2025;177:151469. https://doi.org/10.1016/j.ijhydene.2025.151469.
[5] Navarro MV, Plou J, López JM, Grasa G, Murillo R. Effect of oxidation-reduction cycles on steam-methane reforming kinetics over a nickel-based catalyst. Int J Hydrogen Energy 2019;44:12617–27. https://doi.org/10.1016/j.ijhydene.2018.12.056.
[6] Ding X, Li B, Yang Y, Liu X, Guo Y, Wang Y. Steam reforming of methane over nickel-aluminum spinel-derived catalyst. Int J Hydrogen Energy 2024;51:1256–66. https://doi.org/10.1016/j.ijhydene.2023.09.167.
[7] Lin Y, Wang Z, Tang L, Jiang S, Guo Y, Liu X. Support effect in Ni-based catalysts for methane steam reforming: role of MxOy-Al2O3 (M = Ni, Mg, Co) supports for enhanced catalyst stability. Fuel Process Technol 2025;278:108325. https://doi.org/10.1016/j.fuproc.2025.108325.
[8] Karakache SB, Rouabah M, Gosselin R, Abatzoglou N, Achouri IE. Experimental study and statistical analysis of hydrogen yield in methane steam reforming over a hydroxyapatite-supported nickel catalyst. Catal Today 2025;456:115322. https://doi.org/10.1016/j.cattod.2025.115322.
[9] Garbarino G, Pugliese F, Cavattoni T, Busca G, Costamagna P. A study on CO2 methanation and steam methane reforming over commercial Ni/Calcium aluminate catalysts. Energies 2020;13:2792. https://doi.org/10.3390/en13112792.
[10] Salahi F, Zarei-Jelyani F, Esmaeilzadeh M, Rahimpour MR. Investigating the effect of nickel active site position and synthesis method on performance of Ni-La-Al2O3 catalyst in the steam reforming of methane: optimization by Box Behnken Design (BBD). J Energy Inst 2025;122:102183. https://doi.org/10.1016/j.joei.2025.102183.
[11] De Giacinto A, Tusini E, Doronkin DE, Reguer S, Popescu R, Grunwaldt J-D, et al. Role of Mg:Al ratio and Pt promotion on mitigating the deactivation of Ni-based methane steam reforming catalysts. Appl Catal B Environ Energy 2026;385:126305. https://doi.org/10.1016/j.apcatb.2025.126305.
[12] Jiang MR, Huang MH, Wang SF. Design of an anti-coking and long-lifetime CeO2–NiO–La2O3 catalyst for steam methane reforming. Int J Hydrogen Energy 2025;196:152486. https://doi.org/10.1016/j.ijhydene.2025.152486.
[13] Seong G, Yoko A, Tomai T, Adschiri T. Facet-engineered Pt/CeO2 oxygen carriers for efficient low-temperature chemical looping steam methane reforming. Fuel 2026;407:137406. https://doi.org/10.1016/j.fuel.2025.137406.
[14] Tusini E, Casapu M, Zimina A, Doronkin DE, Störmer H, Barthe L, et al. Structural changes of Ni and Ni–Pt methane steam reforming catalysts during activation,

reaction, and deactivation under dynamic reaction conditions. ACS Catal 2024;14:7463–77. https://doi.org/10.1021/acscatal.3c05847.
[15] Guo X, Xiao Z, Zou J-J, Li G, Wang D. Comprehensive review of catalyst structures and reactor designs for efficient hydrogen production via steam reforming of methane. J Environ Chem Eng 2026;14:120541. https://doi.org/10.1016/j.jece.2025.120541.
[16] Alrshdan MM, Ahmed U, Elserfy K, Nemitallah MA. Hydrogen production through intensified steam methane reforming and hydrogen separation in a membrane rector: process modeling, optimization, and scaling-up. Int J Hydrogen Energy 2025;162:150705. https://doi.org/10.1016/j.ijhydene.2025.150705.
[17] Pashchenko D. Experimental investigation of reforming and flow characteristics of a steam methane reformer filled with nickel catalyst of various shapes. Energy Convers Manag 2019;185:465–72. https://doi.org/10.1016/j.enconman.2019.01.103.
[18] Hanson E, Nwakile C, Hammed VO. Carbon capture, utilization, and storage (CCUS) technologies: evaluating the effectiveness of advanced CCUS solutions for reducing CO2 emissions. Results Surf Interfaces 2025;18:100381. https://doi.org/10.1016/j.rsurfi.2024.100381.
[19] Ferella F, Suichies A, Abdelkader BA, Dabhi NK, Werber J, de Lannoy C-F. Ocean alkalinity enhancement using bipolar membrane electrodialysis: technical analysis and cost breakdown of a full-scale plant. Ind Eng Chem Res 2025;64:7085–99. https://doi.org/10.1021/acs.iecr.4c04364.
[20] Agún B, Abánades A. Comprehensive review on dry reforming of methane: challenges and potential for greenhouse gas mitigation. Int J Hydrogen Energy 2025;103:395–414. https://doi.org/10.1016/j.ijhydene.2025.01.160.
[21] Ranjbar A, Rezaei M. Impact of potassium promoter amount in Ni catalysts supported on CaAl4O7 for methane reforming with CO2. Int J Hydrogen Energy 2024;72:360–6. https://doi.org/10.1016/j.ijhydene.2024.05.230.
[22] Li Y, Xu N, Huang Y, Zhang Z, Xu G. The dynamic rapid deactivation-slow reactivation behavior of porousα-Al2O3-supported Ni catalysts in the fluidized-bed dry reforming at extremely high space velocities. Fuel 2026;413:138255. https://doi.org/10.1016/j.fuel.2026.138255.
[23] El-Temtamy SA, Ebiad MA, ElHafiz DRA, El-Salamony RA, Ghoniem SA, Naggar AMA El, et al. Effect of Ni content in Ni-pillared clay catalyst on syngas production from dry reforming of methane at low temperature. Next Res 2025;2:101056. https://doi.org/10.1016/j.nexres.2025.101056.
[24] Huang M, Xu R, Deng L, Zhao G, Jiang D, Si J, et al. Nickel-based core-shell catalysts modified by Ca for dry reforming of methane with high sintering- and coke-resistance. Int J Hydrogen Energy 2026;200:152913. https://doi.org/10.1016/j.ijhydene.2025.152913.
[25] Wang C, Wang C, Xiang L, Gao Y, Qian H, Bi F, et al. Electrothermal-driven nickel-based bifunctional catalyst for robust dry reforming of methane. Appl Catal B Environ Energy 2026;386:126362. https://doi.org/10.1016/j.apcatb.2025.126362.
[26] de Queiros Souza GE, de Andrade Schaffner R, do Nascimento CT, Beraldi Gomes CM, Oliveira LG, Cerutti DL, et al. Evaluation of reaction conditions in the dry reforming process using a Ni/MCM-41 catalyst for syngas production. Int J Hydrogen Energy 2025;158:150503. https://doi.org/10.1016/j.ijhydene.2025.150503.
[27] Córdoba M, Choya A, de Rivas B, Gutiérrez-Ortiz JI, López-Fonseca R. Dry reforming of methane over nickel aluminate-derived catalysts modified with lanthanum and magnesium. Catal Today 2025;460:115483. https://doi.org/10.1016/j.cattod.2025.115483.
[28] Niu Y, Zheng X, Guo B, Liu H, Jin Y, Niu J. Particle size tuning of Ni/CeO2 catalysts and their performance in methane dry reforming reaction. Gas Sci Eng 2026;145:205790. https://doi.org/10.1016/j.jgsce.2025.205790.
[29] Cao Y, Wen P, Wu R, Liu N, Dai C, Chen B. Robust Ni-based FER zeolite catalyst with Mg doping for efficient and stable methane dry reforming. Int J Hydrogen Energy 2026;204:153129. https://doi.org/10.1016/j.ijhydene.2025.153129.
[30] Chanthanumataporn M, Kiatirabil J, Wongsakulphasatch S, Assabumrungrat S. Development of CeO2-coated LaNiO3 perovskite catalyst for enhanced low-temperature dry reforming of methane. Fuel 2026;412:138113. https://doi.org/10.1016/j.fuel.2025.138113.
[31] Liu W, Yuan Q, Xu J, Xie H, Chen S, Zeng J, et al. Construction of the Co/MnO catalyst surface active sites for efficient dry reforming of methane (DRM) at low-temperature. Int J Hydrogen Energy 2026;200:152943. https://doi.org/10.1016/j.ijhydene.2025.152943.
[32] Cordeiro JLC, Safdar M, da Silva JS, de Aquino GS, dos Santos Rios JGV, dos Santos MB, et al. Effect of support on Ni catalysts prepared by the combustion method applied in the dry reforming of biogas for production of sustainable hydrogen. Int J Hydrogen Energy 2026;204:153150. https://doi.org/10.1016/j.ijhydene.2025.153150.
[33] Pasupathi A, Balakrishnan I, Cordier N, Batiot-Dupeyrat C, Bellan S, Mostaghimi J, et al. Synergistic impact of catalyst and tri-cathode thermal plasma torch for efficient dry reforming of CH4 with CO2. Int J Hydrogen Energy 2026;199:152662. https://doi.org/10.1016/j.ijhydene.2025.152662.
[34] Chem LG. LG chem and POSCO holdings join forces for CCU technology demonstration project n.d. https://www.lgcorp.com/media/release/28945. [Accessed 26 February 2026].
[35] Flanders Moonshot. UGent researchers open the groundbreaking super-dry reforming (SDR) pilot plant. https://www.moonshotflanders.be/en/news/ugent-researchers-open-groundbreaking-super-dry-reforming-sdr-pilot-plant. [Accessed 26 February 2026].
[36] Abotaleb A, Abounahia N, Makeen S, Ponraj J, Al Yarabah M, Ferella F, et al. Assessing the recyclability of spent fluid catalytic cracking catalyst for sustainable dry reforming of methane. Fuel 2024;373:132356. https://doi.org/10.1016/j.fuel.2024.132356.
[37] Nogales-Delgado S, González González JF. The role of catalysts in life cycle assessment applied to biogas reforming. Catalysts 2024;14. https://doi.org/10.3390/catal14090592.
[38] Devasahayam S, Thella JS, Mohanty MK. Sustainability assessment of dry reforming of methane via carbon intensity and syngas energy recovery analysis. Energies 2025;18:1–39. https://doi.org/10.3390/en18236307.
[39] Duclos L, Chattot R, Dubau L, Thivel PX, Mandil G, Laforest V, et al. Closing the loop: life cycle assessment and optimization of a PEMFC platinum-based catalyst recycling process. Green Chem 2020;22:1919–33. https://doi.org/10.1039/c9gc03630j.
[40] Bharadwaj AS, Nayak RR, Koteswararao J, Sampath C, Gaddala B, Pawar BG, et al. Environmental life-cycle assessment and green principles in process intensification: a review of novel catalysts from solid waste. Chem Eng Process Intensif 2025;211:110208.
[41] Aromaa-Stubb R, Rinne M, Lundström M. Life cycle assessment of cobalt catalyst production and recycling. J Sustain Metall 2024;10:1795–806.
[42] Trenord. On the tracks of innovation: hydrogen trains. https://www.trenord.it/en/about-us/the-mobility-revolution/the-novelty-of-the-hydrogen/?_gl=1*1567k6j*_up*MQ..*_ga*OTczNjg4MzI1LjE3NzIxMDMwNDg.*_ga_CFQRRL9CP6*czE3NzIxMDMwNDgkbzEkZzAkdDE3NzIxMDMwNDgkajYwJGwwJGgw. [Accessed 26 February 2026].
[43] Thyssengas GmbH. Gasunie and thyssengas sign agreement for first cross-border hydrogen transport infrastructure between the Netherlands and Germany n.d. https://thyssengas.com/en/article/gasunie-and-thyssengas-sign-agreement-for-first-cross-border-hydrogen-transport-infrastructure-between-the-netherlands-and-germany. [Accessed 26 February 2026].
[44] Abotaleb A, Abounahia N, Sinopoli A, Ferella F. Reuse of CO-Oxidation spent catalysts for dry reforming of methane: techno-economic analysis. ACS Sustain Chem Eng 2026;14:1381–94. https://doi.org/10.1021/acssuschemeng.5c09652.
[45] ISO 14044. Environmental management-Life cycle assessment-requirements and guidelines. 2021.
[46] Gad SC. In: Wexler P, Toxicol Encycl, editors. Nickel chloride. fourth ed. Fourth Edition, Oxford: Academic Press; 2024. p. 771–5. https://doi.org/10.1016/B978-0-12-824315-2.00704-1.
[47] Affranchi A, Longo S, Cellura M, Inguanta R, Oliveri L. Life cycle assessment of NiFeP electrodes. a Case Study 2025;119:325–30. https://doi.org/10.3303/CET25119055.
[48] ISO 14040. Environmental management - life cycle assessment - principles and frameworks 2021. 2021.
[49] Schmidt A, Frydendal J. Methods for calculating the environmental benefits of 'green'products. Buy into Environ 2003;30.
[50] Piccinno F, Hischier R, Seeger S, Som C. From laboratory to industrial scale : a scale-up framework for chemical processes in life cycle assessment studies. J Clean Prod 2016;135:1085–97. https://doi.org/10.1016/j.jclepro.2016.06.164.
[51] Bermúdez JM, Beneroso D, Rey-raap N, Arenillas A, Menéndez JA. Chemical engineering and processing : process intensi fi cation energy consumption estimation in the scaling-up of microwave heating processes. Chem Eng Process Process Intensif 2015;95:1–8. https://doi.org/10.1016/j.cep.2015.05.001.
[52] Petrucciani A, Amato A, Norici A, Dibenedetto A, Aresta M. Life cycle assessment of diatom frustule production : a multitask, vol. 92; 2025.